Chemical Industry & Chemical Engineering Quarterly

Available online at
Association of the Chemical Engineers of Serbia AChE
www.ache.org.rs/CICEQ

Chem. Ind. Chem. Eng. Q. 33 (1) xxx–xxx (2027) CI&CEQ

RAJASEKAR SIVASANKARI[1]
https://orcid.org/0009-0005-2248-838X
NALLATHAMBI GOLDEN STEPHA[2]
https://orcid.org/0000-0001-5382-8598

[1]Department of Mathematics, Easwari Engineering College, Chennai, India
[2]Department of Mathematics, R.M.K Engineering College, Gummidipoondi, India

3D FLOW DYNAMICS OF HYBRID NANOFLUID UNDER RADIATION AND ACTIVATION ENERGY

Highlights

- The study focuses on a composite of nanoparticles MgO-TiO_2 applied to a cylindrical surface
- It investigates three-dimensional stagnation flow, including saddle and nodal points
- Concentration profiles are analyzed for a hybrid nanoparticle with activation energy
- The similarity transformation technique is applied to convert the PDEs into ODEs
- MATLAB's bvp4c solver is used to solve the ordinary differential equations (ODEs)

Abstract

This article seeks to study magnetohydrodynamics (MHD) and the porosity of hybrid nanofluid on a three-dimensional stagnation point over the sinusoidal radius of a circular cylinder. The nodal and saddle stagnation points are analysed through graphs for radiation, viscous dissipation, heat transfer, and activation energy employed in mass transfer. With the use of similarity variables, the nonlinear Partial Differential Equation (PDE) was converted to an Ordinary Differential Equation (ODE), which MATLAB's bvp4c solver then resolved. The skin friction and Nusselt number give good agreement with previously published findings pertaining to the saddle and nodal positions at ratios of velocity gradients of -0.5 and 0.5. This study offers a novel analysis of concentration distribution at the boundary layer for a hybrid nanofluid system made up of magnesium oxide (MgO) and titanium dioxide (TiO_2). The significance of activation energy is highlighted, as its influence on the concentration distribution in the stagnation point flow of hybrid nanofluid has not been thoroughly investigated in previous studies. Graphical representations are provided for the effects of MHD, porosity, radiation, viscous dissipation, and activation energy on temperature, velocity, and concentration of fluid flow.

Keywords: circular cylinder, three-dimensional flow, combined MgO-TiO_2 nanofluid, thermal and mass transfer, porous with viscous dissipation.

SCIENTIFIC PAPER

UDC

INTRODUCTION

The cylindrical stagnation point with boundary layer characteristics is very important in industrial thermodynamics applications. These concepts are useful in aircraft noses, hydraulic cylinders, and engine pistons. On account of mechanical interaction and aerodynamic friction, these bodies produce more heat; therefore, effective thermal management is necessary for longevity and outstanding performance.

Nanotechnology applications have grown significantly in fields like heating and cooling, the automotive, biomedical, and energy sectors. Particular uses include lubricants, nanofluids for shock absorbers and automobile brake fluids, nanodrugs, cancer treatment, solar panels, preserving energy, solar absorption, heat transfer mechanisms, aerospace, and defense. The nanofluids are obtained by dispersing nanometer-sized particles in a conventional base fluid, which also enhances their thermal properties. Nanofluids have a single nanoparticle in a base fluid, whereas combining no fewer than two nanoparticles dispersed into a base fluid improves heat transfer

Correspondence: N. Golden Stepha, Department of Mathematics, R.M.K Engineering College, Kavaraipettai, Gummidipoondi, India.
Email: thinkmathematics2020@gmail.com
Paper received: 10 December 2025
Paper revised: 4 May 2026
Paper accepted: 11 June 2026

https://doi.org/10.2298/CICEQ251210006S

capabilities and is termed a hybrid nanofluid. It enhances thermal enhancement and stability at the boundaries. The hybrid nanofluid has a wide range of applications, like heat exchangers, natural convection enclosures, photovoltaic modules, heat sinks, boiling applications, thermal energy storage systems, and heat pipes [1,2]. When calculating the performance of jet engines, the stagnation fluid temperatures and stagnation forces are helpful.

Cylindrical surface bodies have proficient heat transfer capabilities. As a result, it is employed in numerous technical applications involving mass and heat transport. Generally, it is used in chemical reactors, heat exchangers, and electronic cooling systems, which are explored by Reddy and Chamkha [3]. The word nano was first introduced by Choi and Eastman [4], and it has been studied by many researchers and scientists. The nanofluid is a nano-sized particle that is submerged in a base fluid. Nanofluids have good thermal mobility, so this process is deployed to enhance heat transfer in the boundary layer. Many theoretical and experimental reports are given based on this fluid. Li and Peterson [5] explored the thermal emission of aluminium oxide (Al_2O_3) nanoparticles in a base fluid. Buongiorno [6] discussed the effects of thermophoresis and Brownian motion processes affecting heat and mass transport in nanofluids. A few researchers have been carrying out studies of the thermal conductivity and viscosity of nanoparticles with a base fluid. They demonstrate the manner in which the thermal conductivity rose as a result of several influences, including temperature, stability, particle size, and volume fraction ratio. They have concluded that thermal conductivity is increased by adding nanoparticles into conventional fluid [7,8].

Hybrid nanofluids are essential to research and engineering. They further improve the heat transfer and reliability of the boundary layer. Awan *et al.* [9] reported the hybrid nanofluid flow on the stretching cylinder in the presence of Darcy-Forchheimer and magnetic effects. The velocity profile and thermal field are investigated in mono and hybrid nanofluid flow. They observed that the energy is improved because of the Biot number and thermal radiation. Raizah *et al.* [10] explored the three-dimensional hybrid nanoparticles (Ag-MgO) in a circular cylinder with chemical reaction. They concluded that the energy transfer rate increased at the nodal point, causing increased nanoparticle concentration in the base fluid. Fatima *et al.* [11] revealed that hybrid nanofluids can improve cooling and energy transport in rotating systems when paired with advanced heat transfer models. These results have applications in the design of effective cooling systems for mechanical, aeronautical, and energy systems, where exact temperature control is essential. Steady laminar bioconvective magnetohydrodynamics (MHD) flow of a water-based hybrid nanofluid including silver (Ag) and alumina oxide (Al_2O_3) nanoparticles over a moving thin needle in a porous medium with gyrotactic microorganisms was described by Das *et al.* [12]. The experimental study of the thermophysical characteristics of hybrid nanofluid has been revealed by Fikri *et al.* [13]. They analysed thermal transfer and fluid viscosity using the KD2 Pro Thermal-Analyzer and conclude hybrid nanofluids have good thermal conductivity. Explored two-dimensional incompressible forced convective transfer of energy and mass under radiation exposure and chemical interaction using micropolar nanofluid [14,15].

Additionally, viscous dissipation and radiation heat flux were added to the energy equation, which was then numerically solved using the Runge-Kutta 4th-order approach and the shooting methodology. They came to the conclusion that viscosity and thermophoresis enhanced surface angular rotation. MHD free convection across a vertical cone was exposed to radiation, Soret and Dufour effects, and machine learning and numerical Partial Differential Equation (PDE) solvers were applied to investigate the complex MHD convection in non-Newtonian fluids [16,17].

Recently, many researchers have scrutinized mixed nanofluids for thermal conduction and varying viscosity [18,19]. The impact of radiation on the flux of MHD into the combination of Cu-Al_2O_3 nanofluid with base fluid across the stretching/shrinking sheet was examined by Lund *et al.* [20]. Ramesh *et al.* [21] studied the thermophoretic particle deposition and thermal radiation, with a stagnation point on the hybrid carbon nanotubes. The governing equation solved using the Runge-Kutta-Fehlberg (denoted RKF-45) method, and the graph was demonstrated using bvp4c MATLAB. Alsaadi *et al.* [22] examined the effects of mixed convection Arrhenius activation energy on the rate of entropy generation in the presence of porous media. The two-dimensional incompressible non-Newtonian nanofluid flow over a stretching sheet, accounting for thermophoresis and chemical reaction, was analyzed by [23]. The Arrhenius activation energy in heat and mass transfer of second-grade active and passive controls of nanoparticles with the concentration profile was reported by Kalaivanan *et al.* [24]. With entropy optimization, Haya *et al.* [25] investigated the Ree-Eyring nanofluid flow through two spinning disks while accounting for viscosity dissipation and temperature source/sink. They examined the higher activation energy drops in the Arrhenius function, which stimulates the production of chemical reactions. Ramzan *et al.* [26] consciously identified the problem of three-dimensional Darcy-Forchheimer with Williamson nanofluid flow. They explored the heat flux on Fick's laws and also explained the velocity profile on the Hartman number. Nayak *et al.* [27] studied the 3-dimensional free convective flow with the influence of radioactive nanofluid and magnetic field. Nowadays, many researchers have investigated the problem in the three-dimensional steady and unsteady flow for MHD, activation energy, and radiation effects [28,29].

The stagnation point of the 2-dimensional with axisymmetric flow on mass and energy effects has been explored in detail in that literature [30-35]. This research has been triggered to focus on the essentials of the boundary layer flow at the stagnation point by the precise applicability of similarity solutions and their significance to the body's nose and leading edge regions during high-speed flight. The axisymmetric and two-dimensional cases are treated as special cases of stagnation point flow. Howrath [36] explored the nodal stagnation point in three-

dimensional laminar incompressible boundary layer flow and the boundary layer flow on the saddle stagnation point by Davey [37]. Libby [38] investigated the three-dimensional flow of heat and mass transfer over a stagnation point and found a result in nodal and saddle stagnation of the asymptotic solution of uniqueness and non-uniqueness, which was also analyzed numerically. Nowadays, a numerous applications in stagnation point flow, including cooling of electronic devices, hydrodynamic processes, cooling of underground electric cables, polymer extrusion, and geothermal energy extraction. The stagnation fluid temperatures and stagnation forces are useful in jet engine performance calculations. The viscous incompressible liquids on stagnation point flow have been investigated in a wide range of industrial applications. Further, this application has been used in plasma blood flow problems, plastic sheets, cooling of nuclear reactors, and artificial fibres. Bhattacharyya and Gupta [39] and Dinarvand *et al.* [40] investigated the three-dimensional nodal and saddle stagnation points with heat transfer characteristics of electrically conducting and incompressible viscous fluid flow. They found that the boundary layer flow allowed the magnetic field to travel transversely, which is essential in both a theoretical and practical perspective. Such flows are essential in kinetics and forced convective heat transfer. These findings have further practical applications, particularly in manufacturing processes, such as aerodynamic extrusion and nuclear reactor cooling.

The improved performance of a magnesium oxide (MgO) and titanium dioxide (TiO_2) composite applied to a cylindrical surface is highlighted in this work. The MgO-TiO_2 composite is outstanding for minimizing activation energy barriers, which promotes more effective chemical reactions.

Novelty

This study's novel feature is its comprehensive analysis of the flow on a circular cylinder using a hybrid nanofluid composed of MgO and TiO_2. It also examines the effects of magnetic fields, thermal radiation, activation energy, and porous media, as well as the behavior at nodal and saddle stagnation points, which are crucial for fluid flow separation and heat extremes. This integrated model offers a fresh viewpoint on heat and mass transport optimization in advanced cooling, energy, and aerospace systems.

Methodology

Mathematical formulation

The hybrid nanofluid's three-dimensional steady motion in the plane of a revolving cylinder with a radius that varies with sine waves. This system produces a number of stagnation points where the fluid's velocity drops to zero; also, the placement at maximum and minimum radii of the cylinder adds interest to the geometry and influences the boundary layer's evolution.

Fig. 1 depicts the radiation and activation energy flow impact of a three-dimensional hybrid nanofluid model with a sine wave circumference. There are stagnation points *P*, *Q,* and *R* on the cylinder at both the greatest and minimum radii. To divide the upward and downward flow of the cylinder, there are lines from *Q* to *P* and from *Q* to *R*. T_∞ is the uniform temperature of the nanofluid in the environment, and T_W is the temperature of the body surface.

- Point *P* is the origin of a stagnation point.
- *x*-axis: pointing vertically upward
- *y*-axis: along the width of the cylinder
- *z*-axis: normal to the surface

In the inviscid (non-viscous) region near *Q,* as demonstrated by Howrath [36], the velocity elements are:

$$u_e = ax$$

$$v_e = by$$

where a and b are constants related to the free stream, with $|a| \geq |b|$ and a positive.

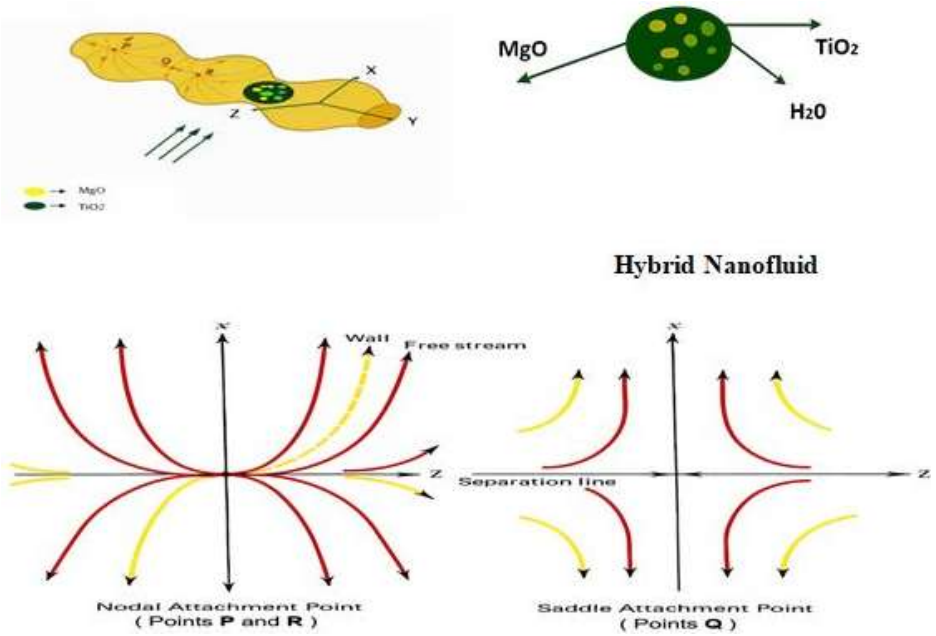

Figure 1: Coordinate system and physical flow configuration of the problem.

Two special cases based on b :

- Plane stagnation flow: $b = 0$ the flow is primarily along one plane.
- Axisymmetric stagnation flow: $b = a$ the flow is radially symmetric around a point.

External streamline pattern

The external (non-viscous) streamlines follow the equation $x_1 = \gamma y^{1/c}$, where $c = b/a$ is the ratio of velocity gradients, and γ is the boundary layer thickness constant.

Depending on c, the flow near the stagnation point classifies into:

Case (i): nodal stagnation point $0 < c \leq 1$

- Streamlines converge smoothly toward the point.
- The flow is stable and directed inward from both x and y directions.

Case (ii): saddle stagnation point $-1 < c \leq 0$

- Streamlines approach from one direction and diverge in another.
- Represents a more unstable flow configuration.

Governing equations [1,2]

The boundary layer equations are:

Continuity equation

$$\frac{\partial u}{\partial x}+\frac{\partial v}{\partial y}+\frac{\partial w}{\partial z}=0 \quad (1)$$

Momentum equation:

$$u\frac{\partial u}{\partial x}+v\frac{\partial u}{\partial y}+w\frac{\partial u}{\partial z}=a^2x+\gamma_{hnf}\frac{\partial^2 u}{\partial z^2}-\frac{\sigma_{hnf}}{\rho_{hnf}}B_0^2u-\frac{\mu_{hnf}}{k}\left(\frac{1}{\rho_{hnf}}\right)u \quad (2)$$

$$u\frac{\partial v}{\partial x}+v\frac{\partial v}{\partial y}+w\frac{\partial v}{\partial z}=b^2y+\gamma_{hnf}\frac{\partial^2 v}{\partial z^2}-\frac{\sigma_{hnf}}{\rho_{hnf}}B_0^2v-\frac{\mu_{hnf}}{k}\left(\frac{1}{\rho_{hnf}}\right)v \quad (3)$$

where u, v, and w represent the velocity components along the x, y, and z directions, respectively. whereas, a and b represent the free stream-dependent constants. The terms ρ_{hnf}, σ_{hnf}, γ_{hnf}, and μ_{hnf} are the density, electrical conductivity, kinematic viscosity, and dynamic viscosity of the hybrid nanofluid, respectively. B_0 is the magnetic field strength, and k_p is the permeability of the porous medium.

Energy equation:

$$u\frac{\partial T}{\partial x}+v\frac{\partial T}{\partial y}+w\frac{\partial T}{\partial z}=\alpha_{hnf}\frac{\partial^2 T}{\partial z^2}+\frac{1}{(\rho C_p)_{hnf}}\frac{16\sigma_1 T_\infty^3}{3k'}\left(\frac{\partial^2 T}{\partial z^2}\right)+\frac{\mu_{hnf}}{(\rho C_p)_{hnf}}\left[\left(\frac{\partial u}{\partial z}\right)^2+\left(\frac{\partial v}{\partial z}\right)^2\right] \quad (4)$$

where T stands for temperature. α_{hnf} and $(\rho C_p)_{hnf}$ are the thermal diffusivity and heat capacity of the hybrid nanofluid. The term σ_1 is the Stefan-Boltzmann constant, and k' is the absorption coefficient. T_∞ is the ambient stream temperature.

Concentration equation:

$$u\frac{\partial C}{\partial x}+v\frac{\partial C}{\partial y}+w\frac{\partial C}{\partial z}=D_{hnf}\frac{\partial^2 C}{\partial z^2}-(C-C_\infty)K_r^2\left(\frac{T}{T_\infty}\right)^n e^{-\frac{E_a}{KT}} \quad (5)$$

where C is the concentration, D_{hnf} is the mass diffusion of hybrid nanofluid, C_∞ is the ambient stream concentration, K_r^2 is the reaction rate, E_a is the activation energy, and $\left(\frac{T}{T_\infty}\right)^n e^{-\frac{E_a}{RT}}$ is the modified Arrhenius function.

Subject to the boundary conditions

$$u=0, v=0, w=0, T=T_W, C=C_W \ \ at \ \ z=0$$
$$u\to u_e, v\to v_e, T\to T_\infty, C\to C_\infty, \ \ as \ \ z\to\infty \quad (6)$$

where T_W and C_W represent temperature and concentration at the wall. u_e and v_e represent free-stream velocity in the x and y direction. Table 1 provides thermophysical properties of hybrid nanofluid.

Non-dimensionalization

Similarity variables

By using the following similarity variables [36]:

$$u=axf'(\eta),\ v=byg'(\eta)$$
$$w=-\left(a\gamma_f\right)^{1/2}\left(f(\eta)+cg(\eta)\right)$$
$$\eta=z\left(\frac{a}{\gamma_f}\right)^{\frac{1}{2}}$$
$$\theta(\eta)=\frac{(T-T_\infty)}{(T_W-T_\infty)}$$
$$\chi(\eta)=\frac{(C-C_\infty)}{(C_W-C_\infty)} \quad (7)$$

where $f(\eta)$ and $g(\eta)$ are dimensionless stream functions in the x and y direction. $\theta(\eta)$ and $\chi(\eta)$ are the dimensionless temperature and concentration inside the boundary layer.

The similarity variables are substituted into Eq. (1), which is satisfied, and the PDEs are transformed into Ordinary Differential Equations (ODEs) [1,2].

$$\left(\frac{A_1}{A_2}\right)f'''+(f+cg)f''+-f'^2-M\left(\frac{A_3}{A_2}\right)f'-K\left(\frac{A_1}{A_2}\right)f'+1=0 \quad (8)$$

where M, A_1, A_2 and A_3 represent magnetic parameter, the effective dynamic viscosity factor, effective density ratio and the effective electrical conductivity ratio respectively. ρ_f and σ_f are the density and electrical conductivity of the base fluid. ρ_{s1} and φ_1 are the density and volume fraction of the magnesium oxide (MgO) nanoparticles, and ρ_{s2} and φ_2 are the density and volume fraction of the titanium dioxide (TiO_2) nanoparticles.

$$\left(\frac{A_1}{A_2}\right)g''' + (f+cg)g'' - cg'^2 - M\left(\frac{A_3}{A_2}\right)g' - K\left(\frac{A_1}{A_2}\right)g' + c = 0 \quad (9)$$

where $c \equiv b/a$ is the ratio of velocity, and $K = \frac{\gamma_f}{k_p.a}$ is the porosity.

$$(Rd+1)\frac{1}{\Pr}\left(\frac{A_4}{A_5}\right)\theta'' + (f\theta' + cg\theta') + Ec\left(\frac{A_1}{A_5}\right)\left(f''^2 + g''^2\right) = 0 \quad (10)$$

where *Pr* is the Prandtl number, which represents the ratio of momentum diffusivity to thermal diffusivity, *Cp* denotes specific heat , *Ec* is Eckert number, that measures the ratio of the kinetic energy of the fluid to the thermal energy difference and R_d is the term radiation parameter.

$$A_4 = \frac{k_{s2} + 2k_{nf} - 2\phi_2\left(k_{nf} - k_{s2}\right)}{k_{s2} + 2k_{nf} + \phi_2\left(k_{nf} - k_{s2}\right)}$$

$$A_5 = \left[(1-\phi_2)\left\{(1-\phi_1) + \phi_1\frac{\left(\rho C_p\right)_{s1}}{\left(\rho C_p\right)_f}\right\}\right] + \phi_2\frac{\left(\rho C_p\right)_{s2}}{\left(\rho C_p\right)_f}$$

$$(1-\phi_1)^{2.5}(1-\phi_2)^{2.5}\chi'' + Sc(f+cg)\chi' - \beta Sc(1+\delta\theta)^n Exp\left(\frac{-E}{1+\delta\theta}\right)\chi = 0 \quad (11)$$

where *Sc* denotes the Schmidt number, which is the ratio of momentum diffusivity to mass diffusivity, *E*, β and δ represent the activation energy, the curvature parameter and the term temperature difference parameter, respectively.

The equivalent initial and boundary conditions of the above equations are

$$f(0)=0,\ f'(0)=0,\ g(0)=0,\ g'(0)=0,\ \theta(0)=1$$
$$\chi(0)=1\ as\ \eta=0$$
$$f'(\infty)=1,\ g'(\infty)=1,\ \theta(\infty)=0$$
$$\chi(\infty)=0\ as\ \eta\to\infty \quad (12)$$

where η represents the dimensionless similarity variable.

The value $\eta = 0$ corresponds to the surface, while $\eta\to\infty$ represents the free-stream region; $f'(\eta)$ and $g'(\eta)$ are dimensionless radial and tangential velocity functions.

Physical parameters

The local Nusselt number, Sherwood number, and local skin-friction coefficient, which have the following definitions, are the special physical parameters.

$$Nu_x = \frac{xq_w}{k_f\left(T_W - T_\infty\right)}$$

$$Sh_x = \frac{-xj_w}{D_B\left(C_W - C_\infty\right)}$$

$$C_{fx} = \frac{\tau_{wx}}{\rho_f u_w^2}$$

$$C_{fy} = \frac{\tau_{wy}}{\rho_f u_w^2}$$

where τ_{wx} is the shear stress surface in the *x* direction and τ_{wy} represents the shear stress surface in the *y* direction, q_w is the surface heat flux, and the term j_w denotes the mass transfer.

Using the similarity variable (7), one obtains:

$$Nu_x\left(\mathrm{Re}_x\right)^{-\frac{1}{2}} = -\frac{K_{hnf}}{K_f}\theta'(0)$$

$$Sh_x\frac{1}{\left(\mathrm{Re}_x\right)^{\frac{1}{2}}} = -\frac{1}{D_B}\chi'(0)$$

$$\left(\mathrm{Re}_x\right)^{\frac{1}{2}}C_{fx} = \frac{f''(0)}{(1-\phi_1)^{2.5}(1-\phi_2)^{2.5}}$$

$$\left(\mathrm{Re}_x\right)^{\frac{1}{2}}C_{fx} = \frac{f''(0)}{(1-\phi_1)^{2.5}(1-\phi_2)^{2.5}}$$

where Nu_x represents the local Nusselt number, Sh_x denotes the local Sherwood number, and C_f represents the skin friction coefficient. The symbol $\mathrm{Re}_x = \frac{ax^2}{\gamma_f}$ is the local Reynolds number defined based on the characteristic length (*x*). The quantities K_{inf} and K_f denote the thermal conductivity of the hybrid nanofluid and the base fluid, respectively. The functions $f''(0)$, $\theta'(0)$, and $\chi'(0)$ are the derivatives of the dimen-sionless velocity gradient, temperature, and concentration profiles at the surface.

RESULT AND DISCUSSION

The non-linear PDEs, Eqs. (2)-(6), are transformed into ODEs using the similarity transformation method. The resulting system of non-linear ODEs, Eqs. (8)-(11), and Eq. (12), is computed by employing MATLAB's bvp4c solver. The similarity solution turns it into a boundary value problem with non-linear coupled ODEs. With appropriate boundary conditions, the aforementioned equations are addressed numerically for a range of dimensionless parameter values. They include general physical parameters such as the Prandtl number, MHD, Porosity, Radiation parameter, Eckert number, Schmidt number, Hartmann number, and reaction rate. The influence of physical parameters on the fluid's temperature, velocity, and concentration, incorporated with the hybrid nanofluid MgO and TiO_2 of the nodal/saddle point on the boundary layer, is thoroughly explained in this work.

The solution to the problem is illustrated through graphical representations, supported by numerical computations across varying parameter values to facilitate analysis. The flexibility of the mathematical model, incorporating multiple influencing factors, allows for future enhancements and extended research possibilities. The parameters used in the simulations–including the density of the base fluid water(H_2O) 998, the density of the hybrid

nanosolid particle, magnesium oxide (MgO) 3560, titanium dioxide (TiO_2) 4250, the hybrid nanofluid volume fractions

Table 1. Thermophysical properties.

Physical quantity connection [19]				
$\frac{\mu_{hnf}}{\mu_f} = 0.6661$	$\frac{\rho_{hnf}}{\rho_f} = 1.4547$	$\frac{\sigma_{hnf}}{\sigma_f} = 1.2204$	$\frac{K_{hnf}}{K_f} = 0.9589$	$\frac{(\rho C_p)_{hnf}}{(\rho C_p)_f} = 0.9$

Thermal and physical volume [19]				
Characters	$\rho(kg \cdot m^{-3})$	$C_p(J \cdot kg^{-1} \cdot K^{-1})$	$k(W \cdot m^{-1} \cdot K^{-1})$	$\sigma(S \cdot m^{-1})$
Water	997.1	4179	0.6071	5.5 10^{-6}
Magnesium-oxide	3560	955	45	5.392 10^{-7}
Titanium-oxide	4250	686.2	8.9538	0.125

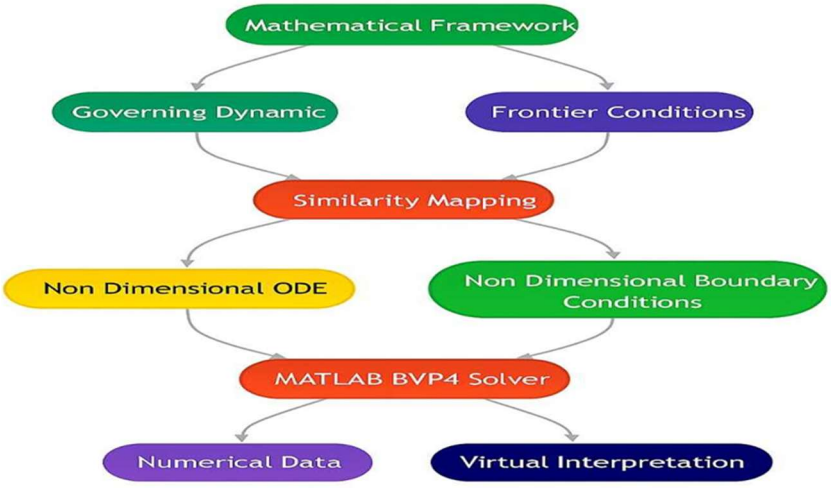

Figure 2: Flowchart representing the methodological framework adopted in this study.

$0.01 < \phi_1 < 0.03$ and $0.01 < \phi_2 < 0.03$, the MHD parameter $1 < M < 3$, the porosity $1 < K < 3$, the radiation parameter $0.5 < N < 1.5$, the Eckert number $0.5 < Ec < 1.5$, the Prandtl number $2.2 < \Pr < 7$, the Schmidt number $0.1 < Sc < 2$, and the activation energy $-1 < E < 1$. Even though the analysis uses default parameter values, investigating different parameter sets provides a more comprehensive understanding and makes it possible to examine a range of physical scenarios within the parameters of the model.

The skin friction coefficient, Nusselt number, and Sherwood number for nodal and saddle points are presented in Tables 2 and 3 for quantitative analysis. Their comparison with existing results from references [1] and [39] demonstrates strong alignment, validating the accuracy and reliability of the present study, as shown in Table 4.

Velocity

Fig. 3(a) and (b) display the velocity distribution of f' and g' for different hybrid nanoparticle volume fractions employing magnesium oxide and titanium oxide, specifically with $c = 0.5$ and $c = -0.5$. As the magnetic field effect (MHD) develops, the velocity profile decreases, as the figure demonstrates. This velocity drop is caused by the Lorentz force, which is applied per unit volume in the electric field. The fluid's dynamics are modified by the impact of this force, which accelerates the flow. Furthermore, the velocity profile obviously drops at a nodal point as the magnetic influence M within the boundary layer increases. Magnetohydrodynamic (MHD) effects increase both temperature and nanoparticle concentration in a fluid; additionally, strong magnetic fields cause redistribution and localized concentration by changing the velocity of nanoparticles. By increasing thermal conductivity, heat is transferred across the flow more effectively. This nodal pattern suggests a distinct transition in which fluid motion is significantly influenced by external factors.

Fig. 3(c) and (d) show that boundary layer velocity reduces at nodal and saddle points while increasing porosity (K), which leads to a thicker boundary layer because of changes in velocity gradients and extended fluid-surface interaction. Higher porosity enhances heat transfer, which gives better fluid absorption, reducing dissipation and raising system temperature, key for controlled heat retention. This promotes uniform flow distribution, stabilizing fluid movement. However, this leads to lower concentration near boundaries due to more even particle dispersion.

Temperature

Fig. 4(a) and 4(b) demonstrate the temperature increases in combination with the hybrid nanofluid volume fractions $\varphi_1 = 0.01$ and $\varphi_2 = 0.02$, respectively. This

increase in the nanoparticle concentration enhances the fluid's capacity to transfer heat, leading to more effective thermal performance. In an effort to improve the distribution of energy in the fluid system, nanoparticles facilitate more effective heat conductivity.

Table 2. Numerical results for the nodal point (c=0.5) on $f''(0)$, $g''(0)$, $-\theta'(0)$, and $-\chi'(0)$ with Pr = 6.2, n = 0.2, and $\varphi_1 = 0.1$.

M	K	N	Ec	Sc	β	δ	E	φ_2	$g''(0)$	$-\theta'(0)$	$-\chi'(0)$
1									0.1005	0.5786	0.3933
2									0.0624	0.5119	0.3753
3									0.0432	0.4522	0.3631
	1								0.1005	0.5786	0.3933
	2								0.0556	0.4941	0.3713
	3								0.0359	0.4197	0.3579
		0.5							0.1005	0.5786	0.3933
		1							0.1005	0.5419	0.3936
		1.5							0.1005	0.5094	0.3939
			0.5						0.1005	0.5786	0.3933
			1						0.1005	0.6265	0.3935
			1.5						0.1005	0.6743	0.3936
				0.1					0.1005	0.5786	0.2452
				0.3					0.1005	0.5786	0.3457
				0.5					0.1005	0.5786	0.3933
					0.0				0.1005	0.5786	0.3740
					0.5				0.1005	0.5786	0.3933
					1.0				0.1005	0.5786	0.3975
						0.0			0.1005	0.5786	0.3960
						0.5			0.1005	0.5786	0.3933
						1.0			0.1005	0.5786	0.3916
							0.0		0.1005	0.5786	0.4005
							0.5		0.1005	0.5786	0.3933
							1.0		0.1005	0.5786	0.3869
								0.01	0.1005	0.5786	0.3933
								0.02	0.1005	0.5786	0.3933
								0.03	0.1005	0.5786	0.3933

Table 3 Impact of the saddle point (c=-0.5) on $f''(0)$, $g''(0)$, $-\theta'(0)$ and $-\chi'(0)$ with Pr = 6.2, n = 0.2, and $\varphi_1 = 0.1$.

M	K	N	Ec	Sc	β	δ	E	φ_2	$g''(0)$	$-\theta'(0)$	$-\chi'(0)$
1									-0.0818	0.5309	0.3916
2									-0.0588	0.4569	0.3755
3									-0.0424	0.3904	0.3640
	1								-0.0818	0.5309	0.3916
	2								-0.0533	0.4369	0.3717
	3								-0.0356	0.3554	0.3590
		0.5							-0.0818	0.5309	0.3916
		1							-0.0818	0.4969	0.3919
		1.5							-0.0818	0.4675	0.3921
			0.5						-0.0818	0.5309	0.3916
			1						-0.0818	0.5318	0.3924
			1.5						-0.0818	0.5327	0.3931
				0.1					-0.0818	0.5309	0.2422
				0.3					-0.0818	0.5309	0.3433
				0.5					-0.0818	0.5309	0.3916
					0.0				-0.0818	0.5309	0.3692
					0.5				-0.0818	0.5309	0.3916
					1.0				-0.0818	0.5309	0.3969
						0.0			-0.0818	0.5309	0.3935
						0.5			-0.0818	0.5309	0.3916
						1.0			-0.0818	0.5309	0.3905
							0.0		-0.0818	0.5309	0.3989
							0.5		-0.0818	0.5309	0.3916
							1.0		-0.0818	0.5309	0.3848
								0.01	-0.0818	0.5309	0.3916
								0.02	-0.0818	0.5309	0.3916
								0.03	-0.0818	0.5309	0.3916

Table 4 Comparison of earlier results with the present study, when Pr = 6.2.

Parameter	c = 0.5	c = 0 .5	c = 0.5
$(\mathrm{Re}_x)^{1/2} C_{fy}$	0.4993	0.4993	0.4739
$(\mathrm{Re}_x)^{-1/2} Nu_x$	1.3302	1.3301	1.2948
Reference	[1]	[39]	Present Study

Furthermore, the figure demonstrates that heat transport is enhanced more by a cylindrical shape than by a flat surface. Heat transfer efficiency is increased because of the increased mixing caused by the cylindrical structure's disruption of fluid flow. Cylindrical shapes are favoured in nanofluid-based systems to improve energy efficiency and heat transfer.

Fig. 4(c) shows that thermal radiation affects temperature. Thermal radiation rises, interacting with the magnetic effect and affecting the surrounding fluid, and enhances the distribution of thermal energy that improves the process. Due to the Stefan-Boltzmann law, the rate of radiation is proportional to the fourth power of temperature, so that the temperature rises while increasing radiation. The greater radiation parameter improves radiative heat transmission, which produces thermal energy. Also, combined conductive and radiative heat transfer raises the temperature of the boundary layer in the nodal stagnation region.

Fig. 4(d) shows that as the Prandtl number increases, the heat transfer process is affected by the boundary layer thickness, which decreases the thermal diffusivity, and the graph indicates the relation of heat transmission and fluid momentum for different Pr numbers. Also, the temperature gradient around the nodal stagnation point increases and is notable.

Fig. 5(a) displays the parameter M increasing, which affects the upper boundary layer and raises heat transport. Because of this, electrically conducting fluid induces magnetic effects within the boundary layer. Additionally, increased MHD changed fluid flow in the boundary layer in the presence of nanoparticles, which changed the temperature gradient.

The temperature profile increases when the porosity K on the boundary layer increases, as shown by Fig. 5(b). So that, the fluid resistance drops, and more heat is absorbed in the region.

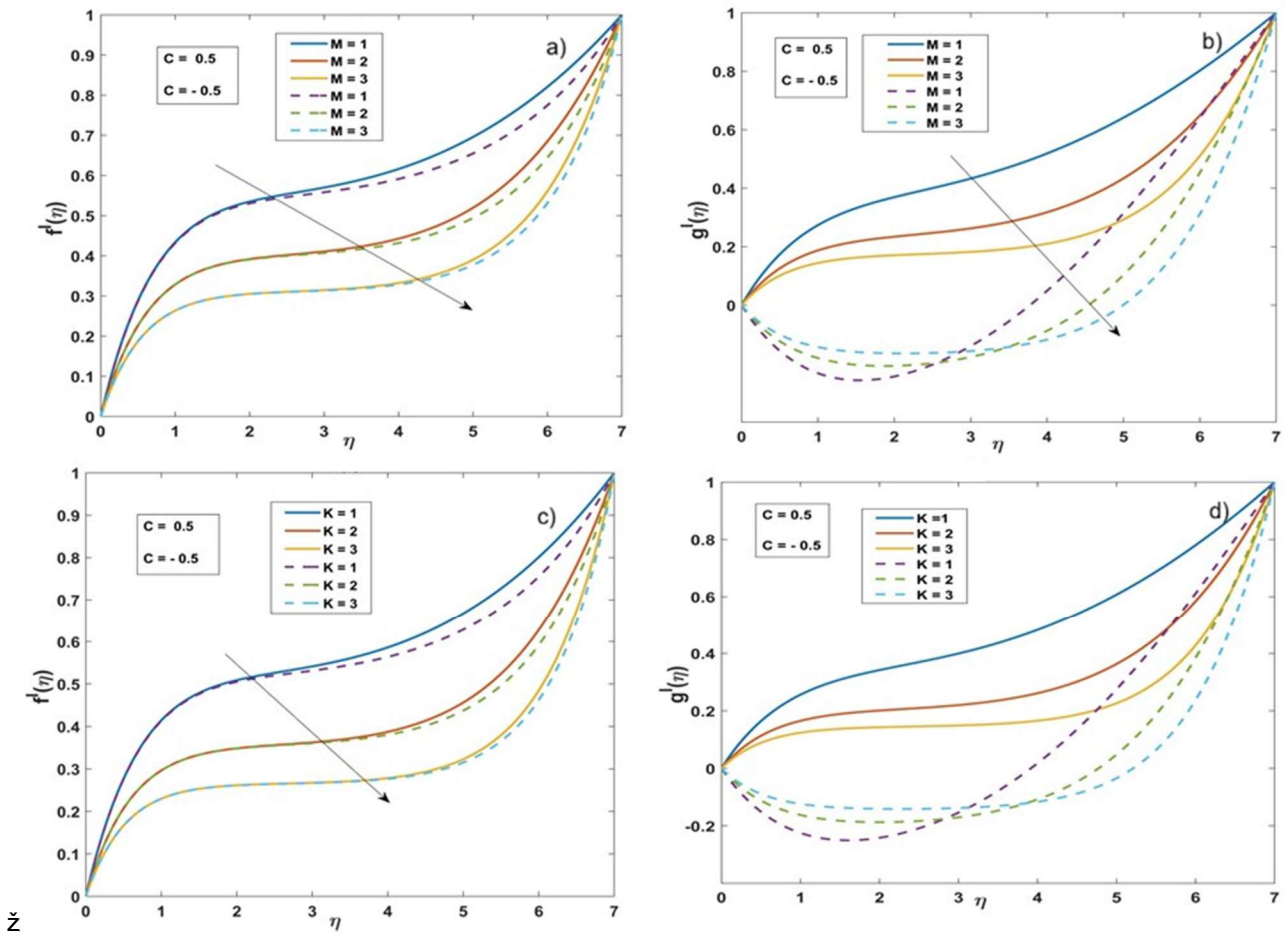

Figure 3: Influence of the magnetic parameter (M) and porosity parameter (K) on the $f'(\eta)$ and $g'(\eta)$ profiles: (a) $f'(\eta)$ versus M, (b) $g'(\eta)$ versus M, (c) $f'(\eta)$ versus K, and (d) $g'(\eta)$ versus K.

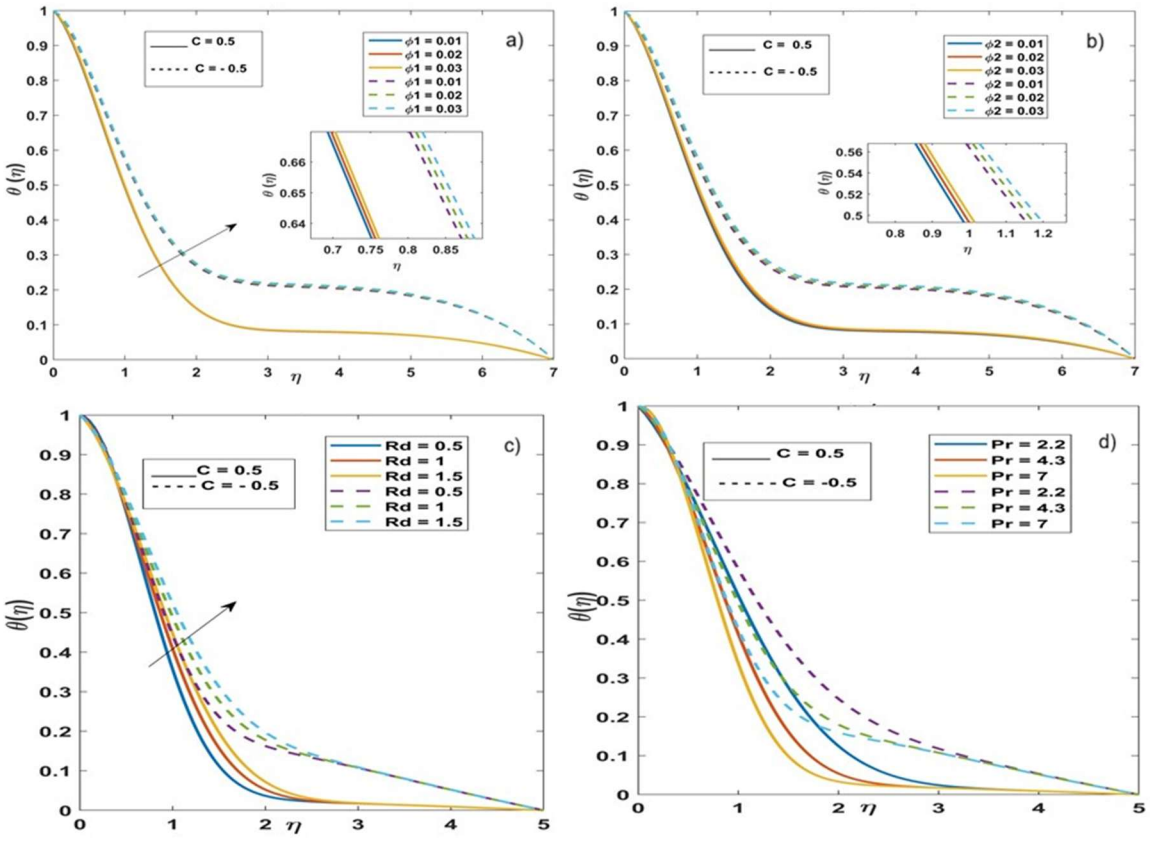

Figure 4: Variation of the temperature profile $\theta(\eta)$ under different effects: (a) nanoparticles φ_1, (b) nanoparticles φ_2, c) radiation parameter, and d) Prandtl number.

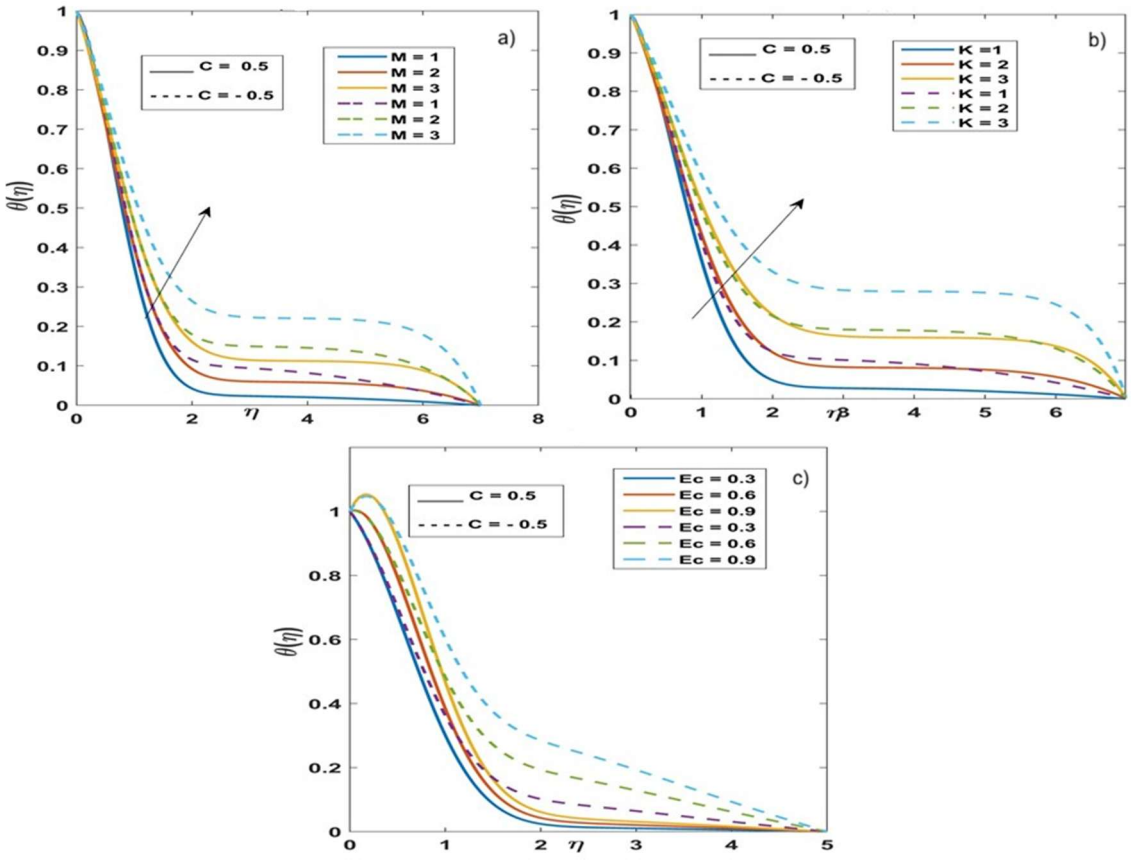

Figure 5: Influence of governing parameters on the temperature profile θ(η): (a) magnetic parameter (M), (b) porosity parameter (K), and (c) Eckert number (Ec).

Fig. 5(c) highlights that increasing the Eckert number (Ec) affects the fluidity of viscosity dissipation, which boosts the boundary layer's overall temperature. Due to the kinetic energy changing to heating energy, this enhanced thermal activity leads to more heat dissipation, particularly on cylindrical surfaces. The temperature increases at the nodal point of the boundary layer and reduces slowly at the free stream. So, the heat accumulates more at the nodal stagnation point. This increased dissipation leads to the boundary layer thickness decreasing, showing a more pronounced thermal gradient.

Concentration

Fig. 6(a) illustrates that Sc affects the concentration distribution of nanofluid particles dissolved in water. The graph indicates that the overall concentration of the nanofluid inside the boundary layer drastically drops as the Schmidt number grows. It has been observed that a greater Schmidt number is associated with a lower concentration in the hybrid nanofluid's boundary layer. Mass diffusion rate is precisely correlated to fluid concentration, while species diffusion decreases as Sc increases. Consequently, the fluid concentration within the boundary layer falls.

Fig. 6(b) and (c) illustrate that as activation energy increases, the reactant particles get sufficient energy to overcome the energy barrier and get involved in the chemical reaction, which reduces the overall reaction rate. Also, the unreacted particles tend to accumulate around nodal and saddle points, leading to a localized increase in concentration. This build-up also contributes to a higher concentration within the boundary layer, as fewer particles are consumed in the reaction and more remain suspended in the flow.

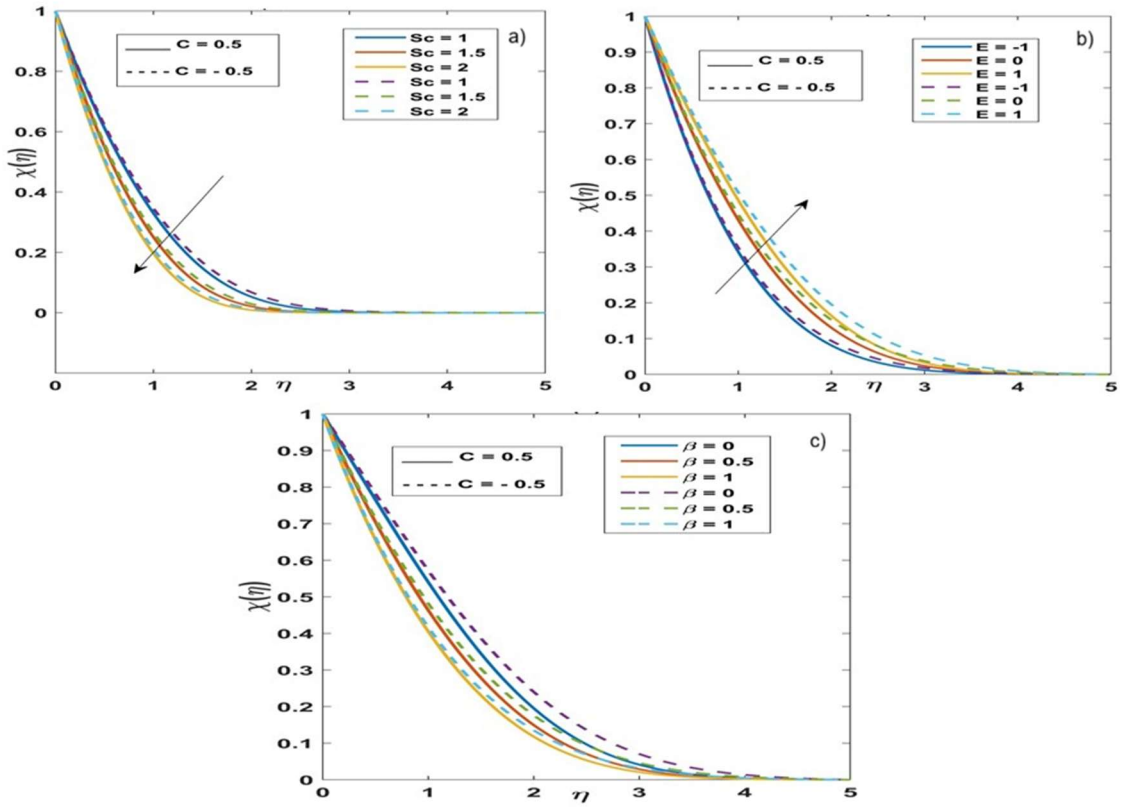

Figure 6: Variation of the concentration profile under different parameters: (a) Schmidt number (Sc), (b) activation energy parameter (E), and (c) β parameter.

CONCLUSION

This study examines the complex behavior of heat and mass transfer involving a combination of MgO and TiO_2 hybrid nanofluid, considering factors such as activation energy, thermal radiation, magnetohydrodynamics (MHD), and porosity, along with graphical representations.

The outcomes provide several important insights:

- The Velocity profile decreases when MHD increases at nodal and saddle stagnation points. The boundary layer flow is more sensitive to magnetic and porous effects.
- Porosity reduces fluid flow velocity and drag force. Due to this, the temperature and concentration of nanoparticles increase at stagnation points.
- The volumetric fraction of nanoparticles enhances heat transfer and thermal conductivity, which disturbs and mixes the fluid flow, giving greater performance on cylindrical surfaces.
- As per the Stefan-Boltzmann law, the radiative energy and thermal radiation improve temperature at the nodal region.
- Higher Pr decreases temperature gradients and thermal diffusivity at stagnation points; also, the

Eckert number increases thermal energy with thickening of the thermal boundary layer.

- Schmidt number (Sc) negatively affects nanoparticle concentration; as Sc increases, mass diffusion drops, reducing concentration in the boundary layer.
- Activation energy reduces reaction rates, allowing more reactants to accumulate, thereby increasing concentration near nodal and saddle regions.

NOMENCLATURE:

a and *b*: Free stream dependent constants
c : Gradient of streamline
C: Species concentration
C_W : Wall concentration
C_∞ Ambient concentration
C_{fx} *and* C_{fy} : Skin friction along x and y direction
Cp: Specific heat (J kg^{-1} K^{-1})
D: Diffusivity
E: Activation energy parameter
E_a : Activation energy
$f(\eta)$: Dimensionless stream function in x direction
$g(\eta)$: Dimensionless stream function in y direction
k: Thermal conductivity (Wm^{-1}K^{-1})
k_r^2 : Reaction rate
Rd: Radiation parameter
Pr: Prandtl number
q_r : Radiative heat flux
Sc: Schmidt number
u_1 and u_2: Free stream velocity
T : Temperature (°C)
T_∞ : Temperature of the fluid at the inlet, (K)
T_W : Constant wall temperature at the surface of the cylinder, (K)
u, v *and* w : Velocity components (m s^{-1})
x, y *and* z : Coordinate axis

GREEK SYMBOLS:

α : Thermal diffusivity
β : Reaction rate
γ : Kinematic viscosity of the fluid, (m^2 s^{-1})
δ : Temperature difference parameter
θ : Dimensionless temperature
μ : Dynamic viscosity of the fluid, (kg m^{-1}s^{-1})
ρ : Density of fluid (kg m^{-3})
σ_1 : Stefan-Boltzmann constant
φ_1 : Volume fraction of nanoparticle (MgO)
φ_2 : Volume fraction of nanoparticle (TiO_2)

SUBSCRIPTS

W : Condition on the wall
∞ : Free stream condition
f: Fluid
s_1 : Solid particle of MgO
s_2 : Solid particle of TiO_2

REFERENCES

[1] S. Dinarvand, Microsyst. Technol. 25 (2019) 2609-2623. https://doi.org/10.1007/s00542-019-04332-3.
[2] S. Nadeem, N. Abbas, A.U. Khan, Results Phys. 8 (2018) 829-835. https://doi.org/10.1016/j.rinp.2018.01.024.
[3] P.S. Reddy, A.J. Chamkha, Ain Shams Eng. J. 9 (2018) 707-716. https://doi.org/10.1016/j.asej.2016.03.015.
[4] S.U.S. Choi, J.A. Eastman, ASME Int. Mech. Eng. Congr. Expo. 17421 (1995) 99-105. https://www.osti.gov/servlets/purl/196525.
[5] C.H. Li, G.P. Peterson, J. Appl. Phys. 101 (2007) 044312. https://doi.org/10.1063/1.2436472.
[6] J. Buongiorno, J. Heat Transf. 128 (2006) 240-250. https://doi.org/10.1115/1.2150834.
[7] D.H. Yoo, K.S. Hong, H.S. Yang, Thermochim. Acta 455 (2007) 66-69. https://doi.org/10.1016/j.tca.2006.12.006.
[8] Y. Zhai, L. Li, J. Wang, Z. Li, Powder Technol. 343 (2019) 215-224. https://doi.org/10.1016/j.powtec.2018.11.051.
[9] A.U. Awan, B. Ali, S.A.A. Shah, M. Oreijah, K. Guedri, S.M. Eldin, Case Stud. Therm. Eng. 49 (2023) 103222. https://doi.org/10.1016/j.csite.2023.103222.
[10] Z. Raizah, A. Saeed, M. Bilal, A.M. Galal, E. Bonyah, Open Phys. 21 (2023) 20220205. https://doi.org/10.1515/phys-2022-0205.
[11] N. Fatima, A. Basem, U. Farooq, M. Imran, M. Tahir, N. Ben Ali, W. Rajhi, H. Waqas, Mech. Time-Depend. Mater. 28 (2024) 1313-1329. https://doi.org/10.1007/s11043-024-09732-1.
[12] U.J. Das, D. Mali, Hybrid Adv. 9 (2025) 100391. https://doi.org/10.1016/j.hybadv.2025.100391.
[13] M.A. Fikri, W.M. Faizal, H.K. Adli, R. Mamat, W.H. Azmi, A.I. Ramadhan, J. Adv. Res. Fluid Mech. Therm. Sci. 108 (2023) 200-214. https://doi.org/10.37934/arfmts.108.2.200214.
[14] N. Golden Stepha, G.N.S. Vijayakumar, K. Muralidharan, Commun. Math. Appl. 14 (2023) 901-914. https://doi.org/10.26713/cma.v14i2.2084.
[15] P. Loganathan, N. Golden Stepha, Asia-Pac. J. Chem. Eng. 8 (2013) 870-879. https://doi.org/10.1002/apj.1732.
[16] S. Varshegaa, P. Francis, P. Sambath, N.A. Ahammad, H.T. Basha, Heat Transf. 54 (2025) 3220-3246. https://doi.org/10.1002/htj.23328.
[17] P. Francis, P. Sambath, S. Noeiaghdam, U. Fernandez-Gamiz, S. Dinarvand, Eng. Sci. Technol. Int. J. 63 (2025). https://doi.org/10.1016/j.jestch.2025.101970.
[18] M.H. Esfe, A.A. Abbasian Arani, M. Rezaie, W.M. Yan, A. Karimipour, Int. Commun. Heat Mass Transf. 66 (2015) 189-195. https://doi.org/10.1016/j.icheatmasstransfer.2015.06.003.
[19] S. Li, S. Akbar, M. Sohail, U. Nazir, A. Singh, M. Alanazi, A.M. Hassan, Case Stud. Therm. Eng. 49

(2023) 103281. https://doi.org/10.1016/j.csite.2023.103281.
[20] L.A. Lund, Z. Omar, I. Khan, E. S.M. Sherif, Symmetry 12 (2020) 276. https://doi.org/10.3390/sym12020276.
[21] G.K. Ramesh, J.K. Madhukesh, N.A. Shah, S. J. Yook, Alex. Eng. J. 61 (2022) 969-979. https://doi.org/10.1016/j.aej.2022.09.026.
[22] F.E. Alsaadi, I. Ullah, T. Hayat, F.E. Alsaadi, J. Therm. Anal. Calorim. 140 (2019) 799-809. https://doi.org/10.1007/s10973-019-08648-0.
[23] N.Golden Stepha, B. G. S. Kumar, G. Swathy, Chem. Ind. Chem. Eng. Q. 30 (2024) 325-333. https://doi.org/10.2298/CICEQ230928005N.
[24] R. Kalaivanan, N.V. Ganesh, Q.M. Al-Mdallal, Case Stud. Therm. Eng. 22 (2020) 100774. https://doi.org/10.1016/j.csite.2020.100774.
[25] T. Hayat, S.A. Khan, M.I. Khan, A. Alsaedi, Comput. Methods Programs Biomed. 177 (2019) 57-68. https://doi.org/10.1016/j.cmpb.2019.05.012.
[26] M. Ramzan, H. Gul, M. Zahri, Bull. Pol. Acad. Sci. Tech. Sci. 68 (2020) 327-335. https://doi.org/10.24425/bpasts.2020.133116.
[27] M.K. Nayak, S. Shaw, A.J. Chamkha, Arab. J. Sci. Eng. 44 (2019) 1269-1282. https://doi.org/10.1007/s13369-018-3473-y.
[28] M. Chaudhry, M. Imran, M. Raza, N. Idrees, Case Stud. Therm. Eng. 73 (2025) 106459. https://doi.org/10.1016/j.csite.2025.106459.
[29] M.M. Syam, M. Alkhedher, M.I. Syam, Int. J. Thermofluids 26 (2025) 101055. https://doi.org/10.1016/j.ijft.2025.101055.
[30] K. Vijayalakshmi, A. Chandulal, H. Alhazmi, A.F. Aljohani, I. Khan, Case Stud. Therm. Eng. 59 (2024) 104457. https://doi.org/10.1016/j.csite.2024.104457.
[31] H.R. Krishna, M.T. Issac, D.D. Ebenezer, Phys. Fluids 35 (2023) 015149. https://doi.org/10.1063/5.0134985.
[32] L.R. Scott, R. Durst, Phys. Fluids 36 (2024) 024118. https://doi.org/10.1063/5.0186496.
[33] A. Cham, M. Mustafa, Case Stud. Therm. Eng. 60 (2024) 104598. https://doi.org/10.1016/j.csite.2024.104598.
[34] U.S. Mahabaleshwar, T. Maranna, M. Mishra, M. Hatami, B. Sunden, Sci. Rep. 14 (2024) 1387. https://doi.org/10.1038/s41598-024-51963-2.
[35] M.N.J. Baig, N. Salamat, F.Z. Duraihem, S. Akhtar, S. Nadeem, J. Alzabut, S. Saleem, Chin. J. Phys. 86 (2023) 1-11. https://doi.org/10.1016/j.cjph.2023.03.017.
[36] L. Howrath, Philos. Mag. 42 (1951) 1433–1440. https://doi.org/10.1080/14786445108560962.
[37] A. Davey, J. Fluid Mech. 10 (1961) 593–610. https://doi.org/10.1017/S0022112061000391.
[38] P.A. Libby, AIAA J. 5 (1967) 507-517. https://doi.org/10.2514/3.4008.
[39] S. Bhattacharyya, A.S. Gupta, Int. J. Non-Linear Mech. 33 (1998) 125-134. https://doi.org/10.1016/S0020-7462(96)00150-3.
[40] S. Dinarvand, R. Hosseini, E. Damangir, I. Pop, Meccanica 48 (2012) 643-652. https://doi.org/10.1007/s11012-012-9621-7.

RAJASEKAR SIVASANKARI[1]
NALLATHAMBI GOLDEN STEPHA[2]

[1]Department of Mathematics, Easwari Engineering College, Chennai, India
[2]Department of Mathematics, R.M.K Engineering College, Gummidipoondi, India

NAUČNI RAD

3D DINAMIKA STRUJANJA HIBRIDNOG NANOFLUIDA POD UTICAJEM ZRAČENJA I AKTIVACIONE ENERGIJE

Ovaj rad ima za cilj ispitivanje magnetohidrodinamike i uticaja poroznosti hibridnog nanofluida pri trodimenzionalnom stagnacionom strujanju preko sinusoidalnog radijusa prethodno razmatranog cilindra. Nodalne i sedlaste stagnacione tačke analizirane su grafički u pogledu uticaja zračenja, viskozne disipacije, prenosa toplote i aktivacione energije koja učestvuje u procesu prenosa mase. Primenom promenljivih sličnosti, nelinearne parcijalne diferencijalne jednačine transformisane su u obične diferencijalne jednačine, koje su zatim rešene pomoću MATLAB rešavača bvp4c. Koeficijent površinskog trenja i Nuseltov broj pokazuju dobro slaganje sa prethodno objavljenim rezultatima koji se odnose na sedlaste i nodalne položaje pri odnosima gradijenata brzine od −0,5 i 0,5. Ova studija pruža novu analizu raspodele koncentracije u graničnom sloju za sistem hibridnog nanofluida sastavljenog od magnezijum-oksida i titan-dioksida. Posebno je istaknut značaj aktivacione energije, budući da njen uticaj na raspodelu koncentracije pri stagnacionom strujanju hibridnih nanofluida nije bio dovoljno detaljno istražen u prethodnim studijama. Grafički su prikazani efekti magnetohidrodinamike, poroznosti, zračenja, viskozne disipacije i aktivacione energije na temperaturu, brzinu i koncentraciju pri strujanju fluida.

Ključne reči: cilindar; trodimenzionalno strujanje; kombinovani MgO-TiO_2 nanofluid; prenos toplote i mase; porozni medijum sa viskoznom disipacijom.